Automated Microrobotic Manipulation of Paper Fiber Bonds*

Juha Hirvonen, Mathias von Essen, Pasi Kallio, *Member, IEEE*

Abstract— **This paper presents a novel method for automated manipulation of individual paper fiber bonds using a microrobotic platform, a computer vision algorithm and a robotic software framework. This is a challenging task due to the three-dimensional, heterogeneous and complex morphology of the fiber bonds. The goal is to automatically grasp the fiber bond, and break it by pulling apart the fibers it consists of. We present the components of the microrobotic platform, and the different rules utilized in detecting suitable grasp points from a 3D reconstruction of the bond generated from an image pair. We demonstrate the functionality of the approach with bond breaking experiments of seven fiber bonds. The time required for grasping and breaking of a bond is 10 – 15 seconds making the approach much faster than the current state-of-the-art testing, which is based on manual manipulation. The success rate of the tests is as high as 80 %.**

I. Introduction

Paper consists mainly of paper fibers, which are chemically or mechanically separated wood cells with a typical length of 1.0 – 4.0 mm and a typical width of 20 – 40 μm [1]. Paper is made in the paper machine by first pressing together the mixture of fibers and water known as pulp and then drying it [2]. This process forms bonds between the adjacent fibers due to the fiber – water interactions and generates a fiber network [1, 2]. The strength of these fiber bonds formed explains mostly the strength of the paper. There has been a lot of research of the methods to measure the bond strength effectively since understanding the factors affecting the bond strength is crucial for making more durable paper [3-9].

Conventionally, physical properties of pulp and paper are tested using hand sheets [10]. However, bond strength cannot be measured with the hand sheets reliably since the mechanical response of the bond cannot be separated from the response of the bonded fiber segments [1]. In order to measure the sole response of the bond, individual fiber bonds have been made by drying two fibers against each other in the way that a bond forms between them. Then, this bond has been broken and the required force has been measured [3-7, 9]. Usually, the bond has been broken by pulling other fiber while the other fiber has been fixed from its both ends. In this paper, we call the fixed fiber as the primary fiber and the pulled fiber as the secondary fiber.

*The research was supported by GETA (Graduate School of Electronics, Telecommunications and Automation) and the Academy of Finland (grant numbers 253364 and 256527).

J. Hirvonen, M. von Essen and P. Kallio are with Department of Automation Science and Engineering, Tampere University of Technology, Korkeakoulunkatu 3, FI-33720 Tampere, Finland (+358 50 300 8154; e-mail: {juha.hirvonen | mathias.vonessen | pasi.kallio}@tut.fi).

Schniewind et al. [3] attached the fiber bonds to rectangular paper strips, whose other end was covered with double-sided adhesive and had a cut in the middle. The ends of the primary fiber were attached to the opposite sides of the cut while the secondary fiber was free in the cut. The paper strip was fixed in the grip of an Instron tensile tester, and the end of the secondary fiber was clamped to the second grip of the tester. The bond was broken by moving the grips apart, and the required force was recorded. A stereomicroscope was used to facilitate handing of the samples.

Stratton and Colson [5] used specially designed Mylar sample holders in their work. The rectangular holder had a U-shaped cut arc in the middle. The primary fiber was fixed laterally over the U from its both ends, and the secondary fiber was fixed longitudinally inside the U from its both ends. Epoxy or hot melt was used in attaching the fibers. The sample holder was then attached to a specially designed measuring device (FLER2). Lateral cuts from the sides of the holder to the upper ends of the U were made to separate the part that held the primary fiber from the part that held the secondary fiber. Then, the parts were pulled apart, and the force needed was measured.

Magnusson and Östlund [6] used a two-part steel sample holder that resembled the holder of [5] after cutting. They glued the ends of the primary fiber to the opposite sides of the cut of the other part, and the other end of the secondary fiber to the cantilever of the other part. The holder was fixed to Instron ElectroPulse E1000 tensile testing machine, and the part with the cantilever was pulled away, and the force needed to break the bond was measured. They also used a FEM model to separate the normal and shear components of the loading.

Fischer et al. [7] also used a sample holder with a somewhat similar principle to [5]. The holder was made of polymer and it was in one part in the beginning. First, the fiber bond was fixed to the holder with nail polish and the holder was attached to the bond tester. Then, the holder was cut either to two or three parts with a soldering rod. The configuration with two parts was similar to [5, 6]. In the configuration with three parts, also the part holding the primary fiber was split in half. This enabled preloading the primary fiber by pulling it to the perpendicular direction before pulling the secondary fiber apart. The bond tester had two load cells to measure the force of the both pulls, and a microscope camera to record the deformation of the fibers during the tests. It is also possible to measure bonding stiffness, bonding energy and shear strength with this setup by using different gluing schemes or sample holder design.

The main problem in all of the presented approaches is the manual fixing of the fiber bond to the sample holder with

glue. This makes the measurement process labor-intensive and time-consuming and the yield is too low to have a statistical importance. To overcome this problem, our research group has developed a microrobotic platform for fiber manipulation and measurements [8, 9]. The advantage of the platform is that its functions can be automated. Bond is broken by first grasping the primary fiber from its both ends with two microgrippers, and then grasping the other end of the secondary fiber with the third microgripper and pulling it apart [8]. The third microgripper should have an integrated force sensor to measure the bond strength. We have shown that it is possible to fabricate such an instrument by using a PVDF film [11]. We have also demonstrated measuring bond strength with the platform by substituting the third gripper with a force sensor and glue [9]. These experiments show the feasibility of breaking the bond by using the microgrippers, and measuring simultaneously the force needed for the breakage.

Microrobotics has been utilized vastly in automated grasping and assembling of industrial microparts [12, 13]. However, there has not been much activity in manipulation of fibrous materials.

We have already demonstrated automated manipulation of individual fibers [14]. In this paper, we demonstrate for the first time automated bond breaking with the platform. The technological novelty of this paper is an algorithm for detecting sufficient grasp points for fiber bond manipulation. We detect the fiber bond placed on the platform by using computer vision, calculate an approximation of its 3D skeleton, and detect the grasp points from the skeleton by applying certain rules. Then, we grasp the bond from those points with the grippers, and break the bond by pulling the secondary fiber. The sensitive gripper is not integrated to the platform yet and hence the bond strength is not measured. However, this work proves that the breaking process can be automated and hence the yield can be increased.

Section II presents the microrobotic platform used in this work, making the fiber bonds for the experiments, and the camera calibration needed for 3D vision. The third section discusses the computer vision algorithm to detect the bonds, to calculate the 3D reconstruction, and to detect the grasp points. The fourth section presents the software for controlling the microrobotic platform. Section V describes the experiments done and the results gained, and Section VI offers the conclusions.

II. Materials and Methods

A. Microrobotic Platform

The microrobotic platform used in the experiments consists of two cameras (AVT, USA) with motorized microscope optics (Navitar, USA), three 3-DOF micromanipulators equipped with microgrippers (SmarAct GmbH, Germany), and a sample stage composed of a rotary stage and an xy stage (both: SmarAct GmbH, Germany). All the actuators are piezoelectric, use the stick-slip principle and have integrated position sensors. The manufacturer-specific control unit performs the low-level control.

The cameras are greyscale, have a resolution of 2452 x 2056 and the maximum frame rate with the highest resolution is 9 fps. The zoom level of the optics can be adjusted between 0.58X and 7.00X, and the nominal width of the images varies correspondingly between 18.97 mm and 1.57 mm. There are also adjustable polarizers in the optics.

The 3-DOF micromanipulators are composed of three linear actuators, and the coordinate axes of the corresponding actuators are parallel apart from small assembly error. The resolution of the actuators is 50 nm.. The microgrippers are named as north, south and west gripper due to their configuration in the platform. There are small dot grids (75 µm dot diameter; 3 x 6, 5 x 4 and 4 x 5 dot configurations with 250 µm spacing) attached to the gripper jaws to facilitate tracking of the grippers in images.

The xy stage and the rotary stage of the sample stage have resolutions of 50 nm and 400 µ°. The sample stage has an integrated illumination system comprised of led elements, a diffuser and a polarizer. The sample holder is made of glass and the illumination system is beneath the holder. A 90° angle between the polarizers of the optics and the polarizer of the illumination system provides high-contrast images where the birefringent paper fibers are seen white on black background. The design of the illumination system is

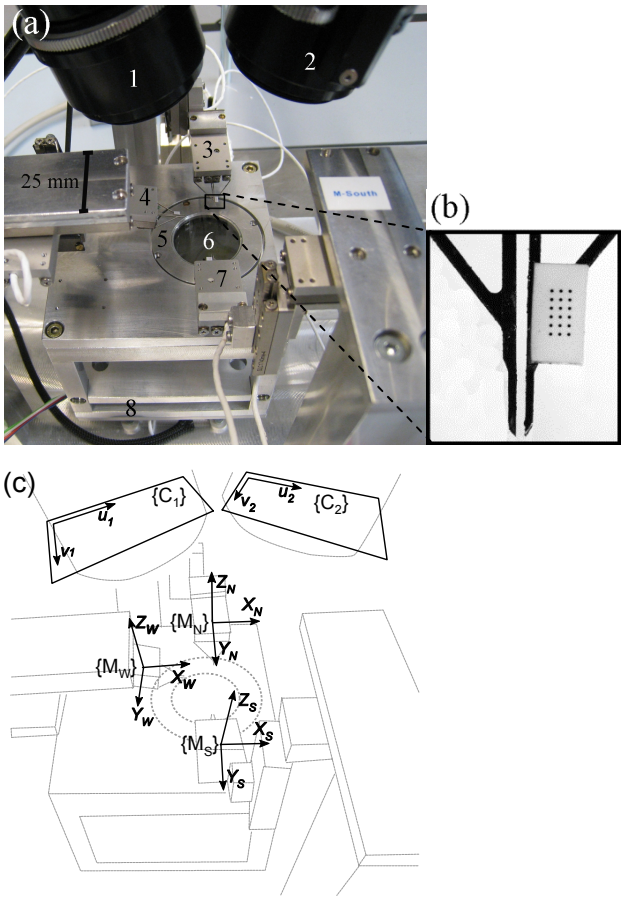

Fig. 1: Microrobotic platform (a): microscope cameras (1, 2), 3-DOF microgrippers (3: north, 4: west, 7: south), rotary stage (5), sample holder (6), and xy stage (8). The north gripper jaws with the dot grid (b). The image planes of its cameras and the frames of the microgrippers (c).

such that the polarizer remains static while the rotary stage is turned. The illumination system is presented with more details in [15]. Fig. 1 shows the microrobotic platform and the coordinate systems of its microgrippers and cameras.

B. Fiber Bonds

We made the fiber bonds for the tests from unbleached softwood kraft pulp. We diluted a portion of pulp to deionized water and pour the solution between two Teflon plates. Then, we put the plates to oven with a 42 N load and let them be in 70˚C for an hour. This caused the fibers crossing each other to bond together. We detected the proper fiber bonds from the plates manually, and moved them to the sample holder of the microrobotic platform by using tweezers.

C. Camera Calibration

The purpose of camera calibration is to generate camera matrices to link the pixel coordinates in the image planes $\{C_1\}$ and $\{C_2\}$ to the manipulator coordinates in the frames $\{M_N\}$, $\{M_S\}$ and $\{M_W\}$. The following applies for the camera matrices

$$^{Cj}\mathbf{m} = {}^{Cj}_{Mn}\mathbf{P}\,{}^{Mn}\mathbf{M}\,, \tag{1}$$

where ${}^{Cj}_{Mn}\mathbf{P}$ is a camera matrix between the image plane of a camera j $\{C_j\}$ and the frame of a manipulator n $\{M_n\}$, $^{Cj}\mathbf{m}$ is a homogeneous image point on the image plane $\{C_j\}$ and $^{Mn}\mathbf{M}$ is a homogeneous 3D point in the frame $\{M_n\}$. $^{Cj}\mathbf{m}$ and $^{Mn}\mathbf{M}$ are defined as

$$^{Cj}\mathbf{m} = \begin{bmatrix} u & v & w \end{bmatrix} \tag{2}$$

$$^{Mn}\mathbf{M} = \begin{bmatrix} X & Y & Z & W \end{bmatrix}, \tag{3}$$

where u and v are the horizontal and vertical pixel coordinates in $\{C_j\}$, X, Y and Z are the 3D coordinates in $\{M_n\}$, and w and W denote the scales. The 3D coordinates of an unknown object in $\{M_n\}$ can be solved by solving $^{Mn}\mathbf{M}$ from the following equation pair when the $^{C1}\mathbf{m} \leftrightarrow {}^{C2}\mathbf{m}$ correspondences are known

$$\begin{cases} {}^{C1}\mathbf{m} = {}^{C1}_{Mn}\mathbf{P}\,{}^{Mn}\mathbf{M} \\ {}^{C2}\mathbf{m} = {}^{C2}_{Mn}\mathbf{P}\,{}^{Mn}\mathbf{M} \end{cases}. \tag{4}$$

A camera matrix can be solved by applying (1) if enough $\boldsymbol{M} \leftrightarrow \boldsymbol{m}$ correspondences are known. The minimum number is six since there are 11 unknowns in $\mathbf{P}$ (a 3 x 4 matrix with 11 independent entries and the scale factor) and each correspondence produces two equations. Yet, it is recommended to use at least 28 correspondences to minimize the effect of noise and detection accuracy [16]. We use similar calibration procedure as described in [14]. We move the manipulators to N different positions, and take images in each position with both cameras. Then, we detect the grid that is attached to the grippers in the images, and use the pixel coordinates of the origin of the grid as $^{C1}\mathbf{m}$ and $^{C2}\mathbf{m}$, and the outputs of the position sensors of the manipulators as $^{MN}\mathbf{M}$, $^{MS}\mathbf{M}$ and $^{MW}\mathbf{M}$. The quality of the camera matrices can be assessed by calculating the reprojection error, which is the difference between the measured pixel coordinates and the theoretical pixel coordinates calculated with (1).

III. Grasp Point Detection Algorithm

This section presents the algorithm that detects sufficient grasp points in the frames of the manipulators from an image pair provided by the cameras of the platform. The algorithm has five steps: preprocessing, sorting and pairing, 3D reconstruction, grasp point search, and alignment and grasping. Each of the steps is presented in its own sub-section.

A. Preprocessing

We first produce binary images from the camera images by using an iterative thresholding method. The method first uses a low global threshold to produce a binary image. Then, it removes trash and other small objects not representing the fiber bond in the image by removing all the 8-connected blobs, which have smaller diameters than D pixels. After this, the original greyscale image is masked with the provided binary image. The threshold is then increased step by step and binary images are produced from the masked image by global thresholding until the resulting binary image contains more than one object. The final binary image is the last image still containing only one object. There are sometimes remarkable changes in the brightness of the bonds in the images, and this method chooses automatically the highest possible threshold for each fiber bond.

After this, the remaining objects are thinned to one-pixel-wide skeletons by using the thinning method described in [17] and the pruning method presented in [18]. The branch points and the end points of each object are detected by using hit-and-miss algorithm and appropriate structuring elements. The number of end points should be four for the skeleton to represent a legal fiber bond. The number of branch points can be one of two depending if the crossing fiber skeleton continues from the same pixel after the crossing or not, but the distance between the branch points should not be higher than the expected maximum fiber width W.

B. Sorting and Pairing

The pixel coordinates in a legal skeleton S should be sorted to two sets F and F' based on which fiber object the pixels belong to. Also, the sets ^{C1}F and ^{C2}F, and $^{C1}F'$ and

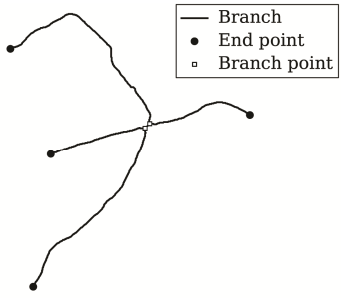

Fig. 2. Skeleton with branches, end points and branch points.

${}^{C2}F'$, should correspond to each other. Therefore, we divide S from its branch point(s) to its four branches B_1, B_2, B_3 and B_4 sorted in the clockwise order around the branch point (or their mean) based on the innermost end point of the branches. Fig. 2 illustrates the branches, end points and branch points of a skeleton. Sorting cannot be based on the end points of S due to different lengths and curliness of the fibers. If there are multiple branch points, we will have also the section between the branch points B_5.Then, we define

$$F = B_1 \cup B_3(\cup B_5), \quad F' = B_2 \cup B_4(\cup B_5) \tag{5}$$

Clockwise sorting is based on the polar coordinates of the points to be ordered. The baseline for the angles is the horizontal of the branch point (or their mean). Due to the different camera views, ${}^{C1}F$ and ${}^{C2}F$ do not necessarily correspond to each other after sorting. However, the difference of projection to image planes $\{C_1\}$ and $\{C_2\}$ is mainly caused by translation since the difference between the camera angles is rather small. This translation t_C is measured during the calibration of the system, and it is utilized in pairing the fibers in different views. Then, for $\forall m \in {}^{C1}F$ we calculate $m - t_c$ and find the nearest neighbor for the result in ${}^{C2}F$ and ${}^{C2}F'$ by using the k-nearest neighbors algorithm. We find the correct $\{C_1\} \leftrightarrow \{C_2\}$ pairs according to the summed distances of the nearest neighbors.

C. 3D Reconstruction

We detect the correspondences between the points in ${}^{C1}F$ – ${}^{C2}F$ and in ${}^{C1}F'$ – ${}^{C2}F'$ as follows. The k-curvature of the fiber skeletons is calculated and then smoothed using a Hanning window. The peaks and troughs of the smoothed k-curvature are detected, and the ones having smaller absolute difference than a set threshold θ to the previous extreme point are discarded. The remaining peaks and troughs are matched between the images by using the cross-correlation of the smoothed k-curvature signals. If more than one point would be matched with the same point, the closest will be matched and the other(s) omitted. Then, the segments between the detected correspondence points are divided to equal number of sections and the section borders are paired together. We calculate the sets of 3D points A and B representing the 3D skeletons of the fibers F and F', respectively, by utilizing (4), the gained ${}^{C1}\mathbf{m} \leftrightarrow {}^{C2}\mathbf{m}$ correspondences, and the camera matrices of one of the microgrippers.

D. Grasp Point Search

We need to find two grasping points from the primary fiber – one on both sides of the bond – and one grasping point from the secondary fiber to be able to grasp the fiber bond and pull it apart. These points are called as primary grasp points and a secondary grasp point, respectively. The sufficient grasp points are searched iteratively from the 3D skeletons representing the fibers. They should fulfill the following conditions:

1. The distance from the bonding point B to the grasp point should be as small as possible to minimize the bending of the fiber during the pull
2. However, the distance from the bonding point to the primary grasp point should be at least d_p to ensure that the bond itself is not grasped, and at least d_s to the secondary grasp point to prevent the west gripper from colliding to the north and south grippers
3. The distance from an adjacent fiber to the grasp point should be at least d_a for the gripper to fit between the fibers
4. The distance from the fiber end point to the grasp point should be at least d_e to enable firm grasping
5. Due to the configuration of the grippers, the grasping sections of the primary points should be nearly parallel to the line connecting the primary points in the xy plane, and the grasping section of the secondary point should be nearly perpendicular to that line in the xy plane. Hence, the β-angles shown in Fig. 3a should be smaller or equal than γ. Grasping section is the part that fits between the jaws and has the length l_{grasp}.

We form two subsets fulfilling Conditions 2, 3 and 4 from the sets A and B: A_{prim}, A_{sec}, B_{prim} and B_{sec}. A_{prim} and B_{prim} contain the points fulfilling the Condition 2 for the primary grasp point, and A_{sec} and B_{sec} contain the points fulfilling Condition 2 for the secondary grasp point. The sets A_{prim} and A_{sec} are defined as follows:

$$A_{prim} = \{\mathbf{M} \in A \,|\, \mathrm{d}(\mathbf{M}, \mathbf{M_b}) \geq d_p, \mathrm{d}(\mathbf{M}, \mathbf{M_e}) \geq d_e, \; \forall \mathbf{M'} \in B : \mathrm{d}(\mathbf{M}, \mathbf{M'}) \geq d_a\} \tag{6}$$

$$A_{sec} = \{\mathbf{M} \in A \,|\, \mathrm{d}(\mathbf{M}, \mathbf{M_b}) \geq d_s, \mathrm{d}(\mathbf{M}, \mathbf{M_e}) \geq d_e, \; \forall \mathbf{M'} \in B : \mathrm{d}(\mathbf{M}, \mathbf{M'}) \geq d_a\}, \tag{7}$$

where $\mathbf{M_b}$ is the bonding point and $\mathbf{M_e}$ is the nearest fiber end point. B_{prim} and B_{sec} are defined similarly.

Now, point combinations of two points from the different sides of the bonding point from A_{prim} and one point from B_{sec} are iteratively tested for Condition 5. This is repeated with B_{prim} and A_{sec}. The β-angles (see Fig. 3a) are calculated until the combination of the primary grasp points $\mathbf{M^p}_i$, i = 1, 2, and the secondary grasp point $\mathbf{M^s}$ that satisfies Condition 5 with the smallest summed distance to the bonding point is detected. Fig. 3 visualizes the conditions, and Fig. 4 shows the steps of the algorithm.

E. Alignment and Grasping

We need to align the bond by using the rotary stage to be able to grasp it with the microgrippers. The primary fiber should be aligned with the north and south gripper, and the secondary point should be in the same side of the bond with the west gripper. We calculate the angle α_0 that the line connecting the primary points forms with the y axis of the north and south gripper. Then, we calculate

$$\mathbf{n}_i^{\mathbf{p}*} = \mathbf{R}^* \mathbf{n}_i^{\mathbf{p}}, \quad \mathbf{n}^{\mathbf{s}*} = \mathbf{R}^* \mathbf{n}^{\mathbf{s}}, \tag{8}$$

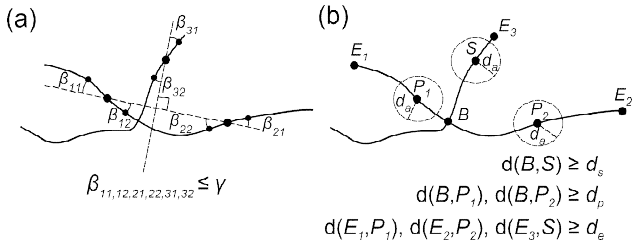

Fig. 3. The conditions grasping points have to fulfill. Straightness conditions (a), and spatial conditions (b).

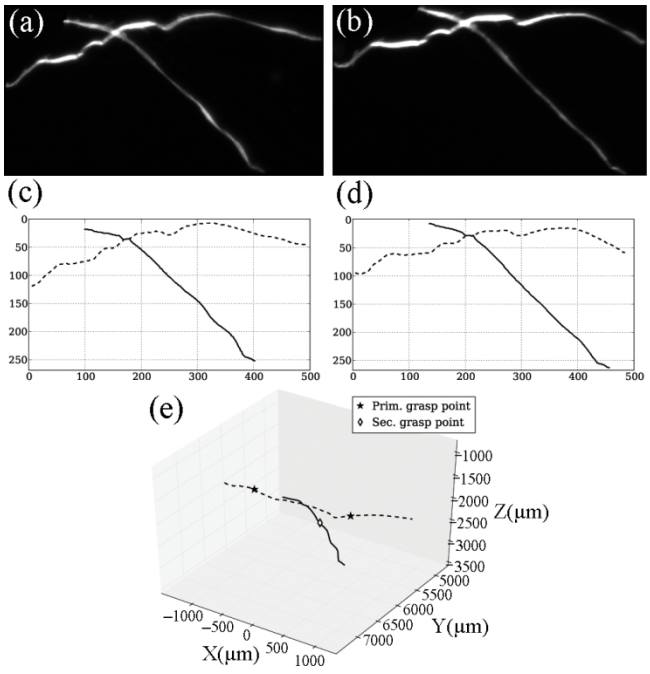

Fig. 4. Steps of the computer vision algorithm. Original images (a, b), paired fiber skeletons (c, d), and the 3D skeleton with the grasp points (e).

where $\mathbf{n}^{\mathbf{p}}_{\mathbf{i}}$ and $\mathbf{n}^{\mathbf{s}}$ contain the xy-plane coordinates of $\mathbf{M}^{\mathbf{p}}_i$ and $\mathbf{M}^{\mathbf{s}}$, $\mathbf{R}^*$ is the 3 x 3 rotation matrix for compensating the angle α_0, and $\mathbf{n}^{\mathbf{p}*}_i$ and $\mathbf{n}^{\mathbf{s}*}$ are the xy coordinates after the rotation. We calculate the final angle α that the rotary stage needs to be turned

$$\alpha = \begin{cases} \alpha_0, & x^{s*} < x_1^{p*} \\ \alpha_0 + \pi, & x^{s*} > x_1^{p*}, \quad \alpha_0 < 0 \\ \alpha_0 - \pi, & x^{s*} > x_1^{p*}, \quad \alpha_0 \geq 0. \end{cases} \tag{9}$$

After the rotation, steps described in Sections IIIA – IIID are applied again, and the 3D skeletons and the grasp points $\mathbf{M}^{\mathbf{p}}_i$ and $\mathbf{M}^{\mathbf{s}}$ are recalculated to get the final grasp points.

Since the 3D skeleton was calculated by using the camera matrices of one of the microgripper, $\mathbf{M}^{\mathbf{p}}_i$ and $\mathbf{M}^{\mathbf{s}}$ are in its frame. We need to transform the grasp points to the frames of the corresponding microgrippers. For example, to transform the coordinates from the frame $\{M_N\}$ to $\{M_W\}$, we first reproject the 3D grasping point coordinates back to the image points:

$$^{C1}\mathbf{m}^{\mathbf{p}}_i = {}^{C1}_{MN}\mathbf{P}^{MN}\mathbf{M}^{\mathbf{p}}_i, \quad ^{C2}\mathbf{m}^{\mathbf{p}}_i = {}^{C2}_{MN}\mathbf{P}^{MN}\mathbf{M}^{\mathbf{p}}_i \ . \tag{10}$$

Then, we solve the following equation pair similarly to (4).

$$\begin{cases} ^{C1}\mathbf{m}^{\mathbf{p}}_i = {}^{C1}_{MW}\mathbf{P}^{MW}\mathbf{M}^{\mathbf{p}}_i \\ ^{C2}\mathbf{m}^{\mathbf{p}}_i = {}^{C2}_{MW}\mathbf{P}^{MW}\mathbf{M}^{\mathbf{p}}_i . \end{cases} \tag{11}$$

IV. Software

The microrobotic platform is controlled with a component-based software that is built on Rock robotic software framework [19]. The motivation behind utilizing a third party software framework is to promote reusability; typical robotic software framework provides a component model, communication middleware and mechanisms to manage the state and the life cycle of the components. Rock relies on Orocos component model that is defined in [20].

The software components utilized in this work can be categorized into low-level hardware interface components and high-level components that implement supportive functionality, algorithms and user interface elements. The low-level components include an off-the-shelf image acquisition component (CameraProsilica), and two in-house developed components (MCSController and NavitarController). MCSController provides the means to communicate with SmarAct's micropositioner controller and NavitarController is responsible for the communication with Navitar's optics. The grasp point detection algorithm is implemented as a high level component that takes images from both cameras as its inputs. The output contains the grasping points for each manipulator in their respective coordinate systems. The automated manipulation tasks are implemented as scripts that orchestrate the run-time behavior of different component instances. More detailed description of the software aspects of the microrobotic platform can be found in [14].

V. Experiments and Results

We solved the camera matrices with each of the actuators by using 32 different positions. The reprojection errors were less than 0.2 pixels for each camera matrix. We also solved the translation t_C by imaging a test target on a sample holder.

We validated the grasp point detection algorithm by using seven different fiber bonds. Table 1 presents the parameters used for the algorithm. We placed the fiber bonds individually onto the sample holder with tweezers. We used the exposure time of 100 ms with the both cameras, and the camera matrices ${}^{C1}_{MN}\mathbf{P}$ and ${}^{C2}_{MN}\mathbf{P}$ in the 3D reconstruction. After the grasp points were detected, the bond was automatically aligned with the grippers, and the grippers were moved to the points with their positioners and closed. Then, the fiber bond was broken by pulling the west gripper for one millimeter. Initially, the grippers were 10 mm above the sample holder, and they were moved to the grasping points axis by axis (ΔX, ΔY, ΔZ). Fig. 5 illustrates the fiber bond grasping procedure.

TABLE 1. PARAMETERS FOR THE GRASP POINT DETECTION ALGORITHM

Parameter Name	Symbol	Value
Low threshold	T	30
Maximum trash diameter	D	100 pix
Maximum fiber width	W	50 µm
Maximum angle in grasping section	Γ	30°
Grasping section length	l_{grasp}	200 µm
Primary point – bonding point distance	d_p	100 µm
Secondary point – bonding point distance	d_s	350 µm
Grasp point – end point distance	d_e	100 µm
Grasp point – adjacent fiber distance	d_a	500 µm

Two of the fiber bonds were classified as ungraspable with the algorithm. Grasping and breaking succeeded with four bonds and failed with one. The cause for the failure was slipping of the secondary fiber from between of the gripper jaws. After the bond was placed onto the sample holder, one test took 10 – 15 seconds.

VI. CONCLUSION

This paper showed for the first time the feasibility of automated fiber bond breaking with microrobotics. The novelty presented was a computer vision algorithm for detecting suitable grasp points from the complex geometry of the fiber bond. We utilized the algorithm and a robotic software framework in controlling the microrobotic platform. We demonstrated that the proposed method is much faster than the manual glue-based procedures commonly used in bond strength testing. Also, the success rate with the bonds recognized as graspable was moderately high (80 %). The gripper with the integrated force sensor will be implemented in the system in the near future to enable measuring the bond strength during the process and hence complete the system. Also, more experiments will be needed to optimize the parameters for the grasp point detection to provide as high yield as possible while still minimizing the error rate. Finally, it is important to ensure that the grasping procedure itself does not cause stress to the bond and affect the measured bond strength. After these improvements, the method will increase throughput in fiber material research.

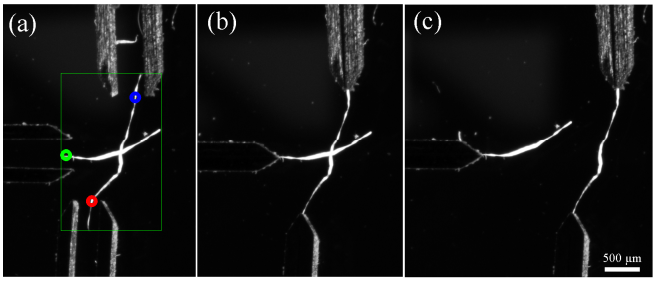

Fig. 5. Fiber bond grasping sequence. Grasping points are detected and the microgrippers are moved to their respective locations (a), microgrippers are closed simultaneously (b), secondary fiber is pulled out to simulate the fiber bond strength measurement (c).

REFERENCES

[1] E. Retulainen, K. Niskanen and N. Nilsen, "Fibers and bonds," in *Paper Physics*, K. Niskanen, Ed. Helsinki, Finland: Fapet Oy, 1998, pp. 55–87.

[2] H. Paulapuro, Ed., *Papermaking Part 1, Stock Preparation and Wet End.* Jyväskylä, Finland: Finnish Paper Engineers' Association, 2008.

[3] A. P. Schniewind, L. J. Nemeth and D. L. Brink, "Fiber and Pulp Properties I. Shear Strength of Single Fiber Crossings," *Tappi J.,* vol. 47, pp. 244, 1964.

[4] T. Uesaka, "Determination of fiber–fiber bond properties," in *Handbook of Physical and Mechanical Testing of Paper and Paperboard*, 2nd ed., R. E. Mark, Ed. New York, USA: Marcel Dekker Inc., 1984, pp. 379–402.

[5] R. A. Stratton and N. L. Colson, "Dependence of fiber/fiber bonding on some papermaking variables," Institute of Paper Science and Technology, Atlanta, GA, USA, IPST Technical Paper Series, 1990.

[6] M. S. Magnusson and S. Östlund, "Inter-fibre bond strength and combined normal and shear loading," in *Progress in Paper Physics Seminar,* Graz, Austria, 2011, pp. 205–207.

[7] W. J. Fischer, U. Hirn, W. Bauer and R. Schennach, "Testing of individual fiber–fiber joints under biaxial load and simultaneous analysis of deformation," *Nord. Pulp Pap. Res. J.,* vol. 27, pp. 237–244, 2012.

[8] P. Saketi and P. Kallio, "Microrobotic platform for making, manipulating and breaking individual paper fiber bonds," in *Assembly and Manufacturing (ISAM), 2011 IEEE International Symposium On,* 2011, pp. 1–6.

[9] P. Saketi and P. Kallio, "Measuring bond strenghts of individual paper fibers using microrobotics," in *Progress in Paper Physics Seminar,* Graz, Austria, 2011, pp. 199–202.

[10] TAPPI Quality and Standards Department, "Physical testing of pulp handsheets," The Technological Association of the Pulp and Paper Industry (TAPPI), GA, USA, Tech. Rep. T-220, 2001.

[11] P. Saketi, S. K. Latifi, J. Hirvonen, S. Rajala, A. Vehkaoja, T. Salpavaara, J. Lekkala and P. Kallio, "PVDF microforce sensor for the measurement of Z-directional strength in paper fiber bonds," *Sensors and Actuators A: Physical,* vol. 222, pp. 194–203, 2/1, 2015.

[12] J. Cecil, D. Powell and D. Vasquez, "Assembly and manipulation of micro devices — A state of the art survey," *Robot. Comput. Integrated Manuf.,* vol. 23, pp. 580–588, 10, 2007.

[13] R. Bogue, "Assembly of 3D micro-components: A review of recent research," *Assem. Autom.,* vol. 31, pp. 309–314, 2011.

[14] M. von Essen, J. Hirvonen, S. Kuikka and P. Kallio, "Robotic software frameworks and software component models in the development of automated handling of individual natural fibers," *J. Micro-Bio Robot.,* vol. 9, pp. 29–45, 2014.

[15] J. Hirvonen, A. Hanninen and P. Kallio, "Design and implementation of an illumination system for microrobotic paper fiber studies," in *Robotics and Automation (ICRA), 2014 IEEE International Conference On,* 2014, pp. 5854–5859.

[16] R. Hartley and A. Zisserman. *Multiple View Geometry in Computer Vision.* NY, USA: Cambridge University Press, 2004.

[17] Z. Guo and R. W. Hall, "Parallel thinning with two-subiteration algorithms," *Commun ACM,* vol. 32, pp. 359–373, 1989.

[18] A. Niemisto, V. Dunmire, O. Yli-Harja, Wei Zhang and I. Shmulevich, "Robust quantification of in vitro angiogenesis through image analysis," *IEEE Trans. Med. Imag.,* vol. 24, pp. 549–553, 2005.

[19] S. Joyeux and J. Albiez, "Robot development: From components to systems," in *6th National Conference on Control Architectures of Robots,* Grenoble, France, 2011, 15 p.

[20] P. Soetens and H. Bruyninckx, "Realtime hybrid task-based control for robots and machine tools," in *Robotics and Automation (ICRA), 2005 IEEE International Conference On,* 2005, pp. 259–264.